Research Article | Vol. 26, No. 5 | 5 Mar 2018 | OPTICS EXPRESS 5225
Optics EXPRESS

Compressive optical interferometry under structural constraints

DAVOOD MARDANI,[1] H. ESAT KONDAKCI,[2] LANE MARTIN,[2] AYMAN F. ABOURADDY,[2] AND GEORGE K. ATIA[1,*]

[1] *Dept. of Electrical and Computer Engineering, University of Central Florida, Orlando, FL 32816, USA*
[2] *CREOL, The College of Optics & Photonics, University of Central Florida, Orlando, FL 32816, USA*
[*] *george.atia@ucf.edu*

Abstract: Compressive sensing (CS) combines data acquisition with compression coding to reduce the number of measurements required to reconstruct a sparse signal. In optics, this usually takes the form of projecting the field onto sequences of random spatial patterns that are selected from an appropriate random ensemble. We show here that CS can be exploited in 'native' optics hardware without introducing added components. Specifically, we show that random sub-Nyquist sampling of an interferogram suffices to reconstruct the field modal structure despite the structural constraints of the measurement system set by its limited degrees of freedom. The distribution of the reduced (and structurally constrained) sensing matrices corresponding to random measurements is provably incoherent and isotropic, which helps us carry out CS successfully. We implement compressive interferometry using a generalized Mach-Zehnder interferometer in which the traditional temporal delay is replaced with a linear transformation corresponding to a fractional transform. By randomly sampling the order of the fractional transform, we efficiently reconstruct the modal content of the input beam in the Hermite-Gaussian and Laguerre-Gaussian bases.

OCIS codes: (260.3160) Interference; (120.3180) Interferometry; (030.4070) Modes.

References and links

1. B. E. A. Saleh and M. C. Teich, *Fundamentals of Photonics* (Wiley, 2007).
2. A. F. Abouraddy, T. M. Yarnall, and B. E. A. Saleh, "Generalized optical interferometry for modal analysis in arbitrary degrees of freedom," Opt. Lett. **37**, 2889–2891 (2012).
3. A. F. Abouraddy, T. M. Yarnall, and B. E. A. Saleh, "Angular and radial mode analyzer for optical beams," Opt. Lett. **36**, 4683–4685 (2011).
4. J. Wang, J. Yang, I. M. Fazal, N. Ahmed, Y. Yan, H. Huang, Y. Ren, Y. Yue, S. Dolinar, M. Tur, and A. E. Willner, "Terabit free-space data transmission employing orbital angular momentum multiplexing," Nat. Photon. **6**, 488–496 (2012).
5. N. Bozinovic, Y. Yue, Y. Ren, M. Tur, P. Kristensen, H. Huang, A. E. Willner, and S. Ramachandran, "Terabit-scale orbital angular momentum mode division multiplexing in fibers," Science **340**, 1545–1548 (2013).
6. D. J. Richardson, J. M. Fini and L. E. Nelson, "Space-division multiplexing in optical fibres," Nat. Photon. **7**, 354–362 (2013).
7. Lluis Torner, Juan P. Torres, and Silvia Carrasco, "Digital spiral imaging," Opt. Express **13**, 873–881 (2005).
8. L. Martin, D. Mardani, H. E. Kondakci, W. D. Larson, S. Shabahang, A. K. Jahromi, T. Malhotra, A. N. Vamivakas, G. K. Atia, and A. F. Abouraddy, "Basis-neutral Hilbert-space analyzers," Sci. Rep. **7**, 44995 (2017).
9. D. L. Donoho, "Compressed sensing," IEEE Trans. Inf. Theory **52**, 1289–1306 (2006).
10. E. J. Candes, "The restricted isometry property and its implications for compressed sensing," C. R. Acad. Sci. **346**, 589–592 (2008).
11. E. J. Candes, "Compressed sensing," Proc. Int. Congress of Mathematicians (2006).
12. M. F. Duarte, M. A. Davenport, D. Takhar, J. N. Laska, T. Sun, K. F. Kelly and R. G. Baraniuk, "Single-pixel imaging via compressive sampling," IEEE Signal Process. Mag. **25**, 83–91 (2008).
13. F. Magalhães, F. M. Araújo, M. V. Correia, M. Abolbashari, and F. Farahi, "Active illumination single-pixel camera based on compressive sensing," Appl. Opt. **50**, 405–414 (2011).
14. L. Martínez-León, P. Clemente, Y. Mori, V. Climent, J. Lancis, and E. Tajahuerce, "Single-pixel digital holography with phase-encoded illumination," Opt. Express **25**, 4975–4984 (2017).
15. P. Clemente, V. Durán, E. Tajahuerce, P. Andrés, V. Climent, and J. Lancis, "Compressive holography with a single-pixel detector," Opt. Lett. **38**, 2524–2527 (2013).

#312604 https://doi.org/10.1364/OE.26.005225
Journal © 2018 Received 2 Nov 2017; revised 10 Jan 2018; accepted 7 Feb 2018; published 21 Feb 2018

Optics EXPRESS

16. B. Deepan, C. Quan, and C. J. Tay, "Compressive sensing for digital holographic interferometry," Proc. SPIE **9234**, 923419 (2014).
17. Y. Rivenson, A. Stern, and J. Rosen, "Reconstruction guarantees for compressive tomographic holography," Opt. Lett. **38**, 2509–2511 (2013).
18. A. Liutkus, D. Martina, S. Popoff, G. Chardon, O. Katz, G. Lerosey, S. Gigan, L. Daudet, and I. Carron, "Imaging with nature: Compressive imaging using a multiply scattering medium," Sci. Rep. **4**, 5552 (2014).
19. C. G. Graff and E. Y. Sidky, "Compressive sensing in medical imaging," Appl. Opt. **54**, C23–C44 (2015).
20. L. Zhu, Y. Chen, J. Liang, Q. Xu, L. Gao, C. Ma, and L. Wang, "Space-and intensity-constrained reconstruction for compressed ultrafast photography," Optica, **3**, 694–697 (2016).
21. M. Süzen, A. Giannoula, and T. Durduran, "Compressed sensing in diffuse optical tomography," Opt. Express **18**, 23676–23690 (2010).
22. R. Yao, Q. Pian, and X. Intes, "Wide-field fluorescence molecular tomography with compressive sensing based preconditioning," Biomed. Opt. Express **6**, 4887–4898 (2015).
23. E. Thiebaut, "Principles of image reconstruction in interferometry," New Concepts in Imaging: Optical and Statistical Models, EAS Publications Series **59**, 157–187 (2013).
24. J. Li, J. S. Li, Y. Y. Pan, and R. Li, "Compressive optical image encryption," Sci. Rep. **5**, 10374 (2015).
25. N. Rawat, B. Kim, I. Muniraj, G. Situ, and B.-G. Lee, "Compressive sensing based robust multispectral double-image encryption," Appl. Opt. **54**, 1782–1793 (2015).
26. Z. Wang and Z. Yu, "Spectral analysis based on compressive sensing in nanophotonic structures," Opt. Express **22**, 25608–25614 (2014).
27. G. A. Howland, J. Schneeloch, D. J. Lum, and J. C. Howell, "Simultaneous measurement of complementary observables with compressive sensing," Phys. Rev. Lett. **112**, 253602 (2014).
28. M. Mirhosseini, O. S. Magaña-Loaiza, S. M. H. Rafsanjani, and R. W. Boyd, "Compressive Direct Measurement of the Quantum Wave Function," Phys. Rev. Lett. **113**, 090402 (2014).
29. A. Kalev, R. L. Kosut and I. H. Deutsch, "Quantum tomography protocols with positivity are compressed sensing protocols," npj Quantum Inf. **1**, 15018 (2015).
30. G. A. Howland, S. H. Knarr, J. Schneeloch, D. J. Lum, and J. C. Howell, "Compressively characterizing high-dimensional entangled states with complementary, random filtering," Phys. Rev. X **6**, 021018 (2016).
31. N. Mohan, I. Stojanovic, W. C. Karl, B. E. A. Saleh, and M. C. Teich, "Compressed sensing in optical coherence tomography," Proc. SPIE **7570**, 75700L (2010).
32. D. Mardani, A. F. Abouraddy, and G. K. Atia, "Efficient modal analysis using compressive optical interferometry," Opt. Express **23**, 28449–28458 (2015).
33. E. Tajahuerce, V. Durán, P. Clemente, E. Irles, F. Soldevila, P. Andrés, and J. Lancis, "Image transmission through dynamic scattering media by single-pixel photodetection," Opt. Express **22**, 16945–16955 (2014).
34. V. Durán, F. Soldevila, E. Irles, P. Clemente, E. Tajahuerce, P. Andrés, and J. Lancis, "Compressive imaging in scattering media," Opt. Express **23**, 14424–14433 (2015).
35. G. Gibson, B. Sun, M. Edgar, D. Phillips, N. Hempler, G. Maker, G. Malcolm, and M. Padgett, "Real-time imaging of methane gas leaks using a single-pixel camera," Opt. Express **25**, 2998–3005 (2017).
36. B. Lawrie and R. Pooser, "Toward real-time quantum imaging with a single pixel camera," Opt. Express **21**, 7549–7559 (2013).
37. D. Starling, I. Storer, and G. Howland, "Compressive sensing spectroscopy with a single pixel camera," Appl. Opt. **55**, 5198–5202 (2016).
38. W. Yu, X. Yao, X. Liu, L. Li, and G. Zhai, "Three-dimensional single-pixel compressive reflectivity imaging based on complementary modulation," Appl. Opt. **54**, 363–367 (2015).
39. G. Howland, P. Dixon, and J. Howell, "Photon-counting compressive sensing laser radar for 3D imaging," Appl. Opt. **50**, 5917–5920 (2011).
40. M. Sun, M. Edgar, D. Phillips, G. Gibson, and M. Padgett, "Improving the signal-to-noise ratio of single-pixel imaging using digital microscanning," Opt. Express **24**, 10476–10485 (2016).
41. Y. Wu, P. Ye, I. Mirza, G. Arce, and D. Prather, "Experimental demonstration of an Optical-Sectioning Compressive Sensing Microscope (CSM)," Opt. Express **18**, 24565–24578 (2010).
42. G. Satat, M. Tancik, and R. Raskar, "Lensless imaging with compressive ultrafast sensing," arXiv, http://arxiv.org/abs/1610.05834 (2016).
43. M. Akhlaghi and A. Dogariu, "Compressive correlation imaging with random illumination," Opt. Lett. **40**, 4464–4467 (2015).
44. D. Xu, N. Vaswani, Y. Huang, and J. Kang, "Modified compressive sensing optical coherence tomography with noise reduction," Opt. Lett. **37**, 4209–4211 (2012).
45. C. Liu, A. Wong, K. Bizheva, P. Fieguth, and H. Bie, "Homotopic, non-local sparse reconstruction of optical coherence tomography imagery," Opt. Express **20**, 10200–10211 (2012).
46. D. Xu, Y. Huang, and J. Kang, "Real-time compressive sensing spectral domain optical coherence tomography," Opt. Lett. **39**, 76–79 (2014).
47. Y. Rivenson, A. Stern, and B. Javidi, "Compressive Fresnel holography," J. Display Technol. **6**, 506–509 (2010).
48. Y. Rivenson, A. Stern, and J. Rosen, "Compressive multiple view projection incoherent holography," Opt. Express **19**, 6109–6118 (2011).

Optics EXPRESS

49. V. Namias, "The fractional Fourier transform and its application in quantum mechanics," IMA J. Appl. Math. **25**, 241–256 (1980).
50. H. M. Ozaktas, Z. Zalevsky, and M. A. Kutay, *The Fractional Fourier Transform with Applications in Optics and Signal Processing* (Wiley, 2001).
51. V. Namias, "Fractionalization of Hankel transforms," IMA J. Appl. Math. **26**, 187–197 (1980).
52. E. Candes and J. Romberg, "Sparsity and incoherence in compressive sampling," Inverse Problems **23**, 969–985 (2007).
53. E. J. Candes and Y. Plan, "A probabilistic and RIPless theory of compressed sensing," IEEE Trans. Inf. Theory **57**, 7235–7254 (2011).
54. J. A. Rodrigo, T. Alieva, and M. L. Calvo, "Programmable two-dimensional optical fractional Fourier processor," Opt. Express **17**, 4976–4983 (2009).
55. K. H. Kagalwala, G. Di Giuseppe, A. F. Abouraddy, and B. E. A. Saleh, "Bell's measure in classical optical coherence," Nat. Photon. **7**, 72–78 (2013).
56. E. Candes, T. Tao, "The dantzig selector: Statistical estimation when p is much larger than n," The Annals of Statistics **35**, 2313–2351 (2007).
57. M. A. Davenport and M. B. Wakin, "Analysis of orthogonal matching pursuit using the restricted isometry property," IEEE Trans. Inf. Theory **56**, 4395–4401 (2010).

1. Introduction

In optical interferometry, an interferogram is typically recorded by sweeping a temporal delay, and the Fourier transform of this interferogram reveals the spectrum [1]. Recently, an interferometric procedure that allows for an optical beam to be analyzed in terms of a complete and orthogonal (but otherwise arbitrary) spatial modal basis has been proposed [2, 3]. Analyzing an optical beam into its constituent spatial modes has direct bearing on numerous applications including spatial-mode multiplexing, quantum communications [4–6], and spiral imaging [7]. The proposed strategy exploits the usual two-path interferometer configuration (such as a Mach-Zhender interferometer, MZI), but replaces the optical delay with a unitary spatial transformation parameterized by a continuous real number that plays the role of a 'generalized delay' in modal space. Akin to temporal interferometry, the Fourier transform of the interferogram – recorded by sweeping the generalized delay – reveals the beam's modal content [2, 3]. This procedure has been realized experimentally for Hermite-Gaussian (HG) and Laguerre-Gaussian (LG) modes in Ref. [8], where the generalized delays correspond to optical implementations of fractional Fourier and fractional Hankel transforms, respectively, realized by spatial light modulators (SLMs). This approach is unique in that the same configuration can be used to analyze a beam in any basis by simply dynamically changing the phase displayed by the SLMs with no moving parts or modification of the optical setup.

In practice, measurements are acquired by sampling the (generalized) delay at the Nyquist rate to avoid aliasing in modal analysis. This requires collecting a large number of samples and implies more latency, which may be intolerable for delay-sensitive applications.

Compressive sensing (CS) is a strategy for reducing the number of measurements required to reconstruct a signal by projecting it onto a basis of (typically) random functions, thereby combining the two steps of *data acquisition* and *compression coding* [9, 10]. This procedure is particularly effective when the signal is *sparse* – i.e., the signal receives contributions from a small number of basis functions in some representation [9]. Underlying this approach is an under-determined linear transformation between the sparse representation and the measurement basis called a *sensing matrix* that is amenable to a stable pseudoinversion [9, 11]. CS has found many uses in optics such as the 'single-pixel' camera [12, 13], holography [14–17], optical imaging and tomography [18–23], optical encryption [24, 25], spectral analysis [26], and efficient quantum state tomography [27–30], and continues to hold promise to impact information recovery in other applications in optics. For example, ultra-fast communications in multi-mode fibers and/or free space using spatial multiplexing of optical modes [4, 5] is premised in part on fast and effective decoding on the receiver side, which can greatly benefit from the relaxed requirement on the number of measurements afforded by CS-based techniques. In Optical Coherence Tomography

Optics EXPRESS

(OCT) [31], CS-based techniques could help reduce complexity in recovering the (normally sparse) reflectivity indices of the different layers of a sample as the spectral coefficients of the reflected optical field, or for complex scene understanding using spiral imaging [7].

Our initial theoretical work [32] proposed a compressive approach to interferometry to reduce the number of interferometric measurements required to faithfully reconstruct the modal weights by exploiting the modal sparsity of beams in typical scenarios. Instead of recording an interferogram sampled uniformly at the Nyquist rate, the number of required samples is significantly reduced by sampling the interferogram at randomly chosen values of the generalized delay and exploiting the linear compressive sensing (CS) model to harness the sparse representation of the beam in modal space. However, no performance guarantees were provided in Ref. [32]. This is a crucial issue considering the fact that, unlike the sensing matrices typically encountered and studied in CS that are drawn from random ensembles, the sensing matrix corresponding to an optical interferometer is highly constrained given the limited number of built-in degrees of freedom of the measurement system. Further, the results provided in Ref. [32] were restricted to numerical simulations. The main contributions of the current paper lie in establishing performance guarantees for successful modal reconstruction at sub-Nyquist sampling rates – most notably under the structural constraints of the measurement system – and realizing the proposed compressive interferometry approach experimentally.

1.1. Related work

CS-based techniques have been instrumental in realizing compression gains in the recovery of sparse signals in numerous applications of optics. The concept of the 'single-pixel' camera originating from applying CS to optical imaging [12, 13], for example, has had notable impacts on holography [14–17], imaging in scattering media [33, 34], imaging gas leaks [35], quantum imaging [36], spectroscopy [37], 3D imaging [38, 39], micro-scanning [40], and microscopy [41]. In this imaging strategy, instead of using a large and expensive CCD or CMOS sampling array, the incident light field is directed towards a Digital Micromirror Device (DMD) – a programmable grid of orientable micro-mirrors. Each micro-mirror pixel reflects the light towards or away from a bucket detector (one with no spatial resolution, hence the 'single-pixel' appellation), such that the measurements amount to a superposition of many pixels weighted by 0 or 1 depending on the orientation of the corresponding micro-mirrors. These coefficients form the entries of an associated sensing matrix, which is a linear transformation that relates the compressive measurements (acquired by the bucket detector) to the multi-dimensional image. By controlling the pattern of the DMD which acts as a spatial mask, one can design favorable sensing matrices to ensure successful signal recovery. Projecting the field onto sequences of random spatial patterns introduced along the optical path as with the single-pixel camera is generally one of the most common CS-based techniques in other applications in optics including quantum state tomography [27, 28, 30].

The recent work in [42] proposed a new lensless imaging system, in which time-resolved and CS-based techniques are combined to reduce the acquisition time for imaging a scene without the need for high-quality lenses and cameras. In this approach, rather than applying random masks to collect the measurements, the target is illuminated with an active pulsed source with different illumination patterns [43]. The measurements are then acquired using an array of time-sensitive sensors placed in the sampling plane. Owing to the use of sensors with high temporal resolution, this approach achieves substantial gains in acquisition time over the more traditional compressive techniques (e.g., the single-pixel camera). In addition, the choice of illumination patterns and control over the temporal resolution of the sensors and their position afford several degrees of freedom in designing appropriate sensing matrices. However, such sampling systems are generally complex and costly.

Other applications in optics leverage CS-based techniques to achieve compression gains only

Optics EXPRESS

in the signal *reconstruction* phase, but *not* in data acquisition. CS-based spectral domain optical coherence tomography (SD-OCT) [31, 44–46] and Fresnel holography [47] are two examples of such applications in which a CCD camera is used to collect a large number of measurements, but only few of them are used for signal recovery using CS-based reconstruction while the rest of the measurements are discarded. For example, in real-time compressive SD-OCT [46], the image recovery is accelerated by utilizing three graphics processing units (GPUs) in a parallel setup to recover the tissue images from a small set of measurements collected by a CCD camera. This method brings about notable speedups in image recovery in comparison to many of the existing CS-based OCT systems, however it uses expensive CCD cameras. Multiple-view projection holography [48] is another domain in which CS has been exploited to address the sensing and recovery complexities involved in 3D imaging. In this approach, a hologram is generated by capturing multiple projections of a 3D scene from different angles using a CCD camera. In that realm, CS recovery algorithms are used to reduce the number of projections required to generate the hologram, thereby relaxing the sensing difficulties associated with the placement of the CCD camera. This approach readily comes with successful reconstruction guarantees – owing to the fact that the rows of the corresponding sensing matrix are samples from the Discrete Fourier Transform matrix (DFT) matrix.

To put the contributions of our paper in context, Table 1 summarizes how the various existing approaches exploit CS in optics in light of the description above, along with properties of the corresponding sensing matrix, and some important features to note when comparing to our proposed approach. Specifically, obtaining random field projections requires modifying the acquisition system by introducing random spatial patterns. The active illumination approach yields significant gains in acquisition time at the expense of additional cost and complexity. Techniques that exploit CS post-acquisition achieve gains only in computational complexity during the reconstruction phase but not in sample complexity since they throw away measurements already collected. We remark that the term 'unconstrained' in the second column of Table 1 (which is a common feature to all previous approaches) should be understood as 'largely unconstrained' to signify that there is much freedom in designing the sensing matrix in the approaches listed. Consequently, the usual CS performance guarantees hold. This is in sharp contrast to our strategy (bottom row in the table) in which the sensing matrix is highly structured with only limited degrees of freedom in the form of a generalized delay parameter. This is a crucial difference where our work differs substantially from previous methods as we have to carry out signal reconstruction under structural sensing constraints set by the optical hardware (a two-path interferometer here) and yet be able to establish some form of performance guarantees.

1.2. Summary of contributions

We underscore four major differences from related work. First, unlike much of the prior work which introduces random masks along the optical path to obtain randomized measurements [14, 30], here we *exploit CS in the native optics hardware* without modification to the underlying interferometer structure nor addition of new hardware components. In other words, we continue to use the same setup and hardware we would use if we were to sample at the full Nyquist rate. As such, we reduce the sampling and reconstruction complexity without increasing the implementation cost. Second, this is the first work to realize compression in the *generalized interferometry* framework introduced recently by some of the authors to carry out modal analysis in arbitrary domains [2, 3, 8]. In this framework, the conventional temporal delay is replaced by a 'generalized delay', namely, a suitable unitary transformation in the form of a fractional transform for which the modal basis elements are eigenfunctions. Third, we achieve compression gains both in the acquisition time and the number of measurements used for reconstruction. This is in sharp contrast to prior works [31, 47] employing CS in optical interferometry, which solely focused on reducing the number of measurements. As we pointed out earlier, in this line of work a large

Optics EXPRESS

Table 1. **Summary of existing approaches in which CS is exploited in optics along with properties of the corresponding sensing matrix. The rightmost column highlights distinguishing features when comparing these approaches to our work. The bottom row refers to our proposed approach studied here.**

Approach	Sensing matrix/structure	Distinguishing features
Random field projections: e.g., using a DMD as a random mask in a single-pixel camera configuration [12, 15]	Random with binary-valued coefficients / unconstrained; e.g., Hadamard matrix	System modification is needed by adding extra hardware components; Gains: reduction in sampling costs and reconstruction complexity
Active illumination: e.g., lensless imaging with structured illumination [42]	Random or designed / unconstrained: e.g., Hadamard patterns; has a large number of degrees of freedom	Costly and difficult to setup; Gains: short sampling time and reduction in reconstruction complexity
Post-acquisition or utilizing high-resolution cameras: e.g., CS-OCT [31]	DFT sub-matrix / unconstrained	Using large high-resolution cameras Gains: reduction only in reconstruction complexity
Basis-neutral approach to generalized interferometry (studied here)	Highly-constrained / structured; rows set by choice of generalized delay parameters	Uses native optics hardware (no additional components); Gains: reduction of acquisition time and reconstruction complexity

number of measurements is first collected using a high-resolution camera. Subsequently, most of the already-collected measurements are discarded and only a few are used for reconstruction on the basis of signal sparsity. While this approach reduces the computational complexity associated with signal reconstruction (fewer measurements are used for recovery), it does not translate into savings in data acquisition time. By contrast, our approach collects a small set of measurements in the first place, thereby achieving the *twin objectives* of reduced sample size and computational complexities. Recalling that we do not modify the interferometric setup from the one used for sampling at the full Nyquist rate, it is not clear at the outset whether the constrained sensing structure lends itself to any form of performance guarantees under sub-Nyquist sampling. Our fourth contribution lies in *establishing analytical guarantees for successful modal reconstruction from compressive measurements under sensing constraints set by the limited degrees of freedom of an optical interferometer*.

We introduce CS into a prototypical optical system – a two-path interferometer – and demonstrate experimentally that sampling the interferogram below the Nyquist rate still enables spectral/modal recovery. We first cast the procedure of interferometric spectral/modal reconstruction as a linear measurement problem. We find that the reduced sensing matrix associated with random sub-Nyquist sampling satisfies sub-optimal conditions of isotropy and incoherence, thereby enabling compressive reconstruction from fewer samples [32]. We denote this overall optical measurement scheme *compressive interferometry* since it combines reduced data acquisition (reduced number of interferometric points sampled) with compressive coding (replacing harmonic analysis with CS reconstruction).

2. Compressive model

For sake of generality, we employ a two-path interferometer in which the usual temporal delay is replaced by a 'generalized delay' that operates in the Hilbert space defined by any modal basis of interest [2, 3]. Such a delay corresponds to an optical transformation that has this modal basis as eigenfunctions, which reduces to the traditional temporal delay when spectral harmonics are of interest. The 'delays' for Hermite-Gaussian (HG) or radial Laguerre-Gaussian (LG) modal

Optics EXPRESS

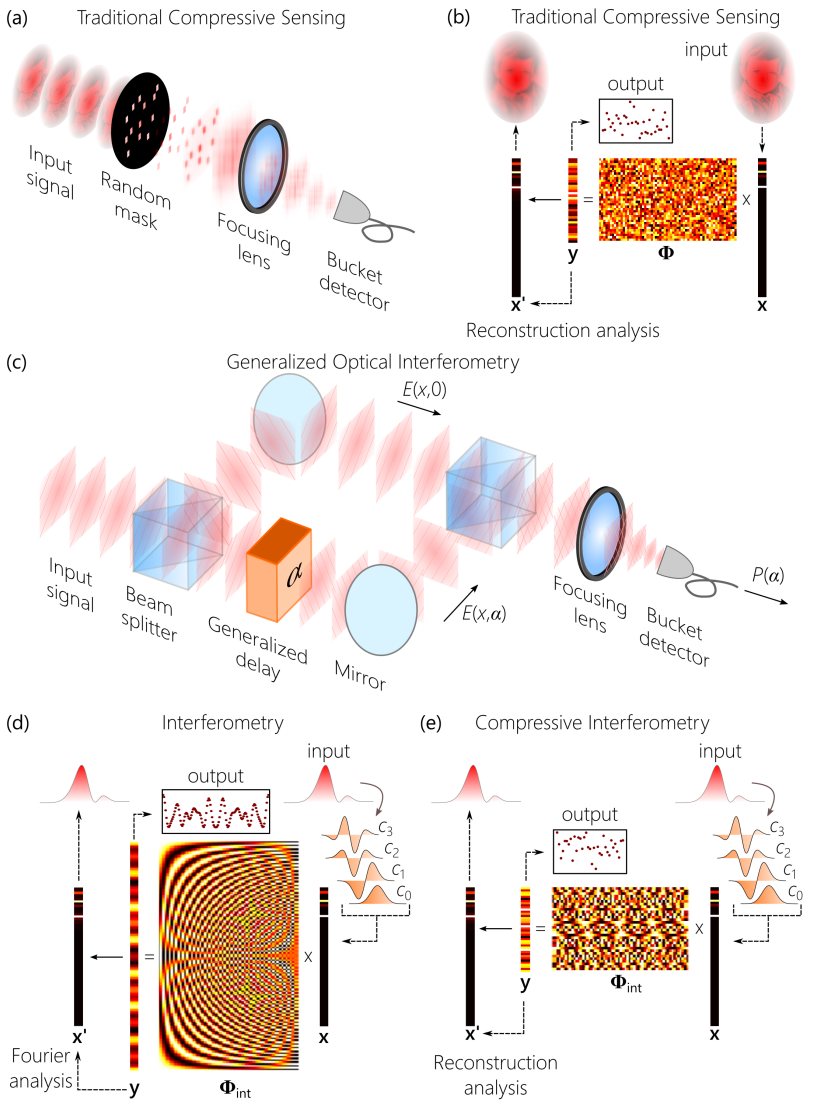

Fig. 1. Concept of compressive optical interferometry. (a) Schematic of the traditional CS scheme in optics, where the field $E(x)$ is subject to random projections before measurements. (b) The mathematical concept used in traditional CS. The field is represented by a $M\times1$ vector $\mathbf{x}$ that is transformed by a $M\times N$ sensing matrix $\mathbf{\Phi}$ (with disordered entries corresponding to the random masks) to yield a $M\times1$ measurement vector $\mathbf{y}$, from which $\mathbf{x}$ is reconstructed. (c) The generalized interferometry scheme. The input beam $E(x)$ is directed to a Mach-Zhender interferometer in which a generalized delay α replaces the usual temporal delay. Two copies of $E(x)$ are created at a beam splitter and the modes $\{\psi_n(x)\}$ underlying the beam acquire phase shifts of the form $e^{in\alpha}$ after passing through the generalized delay to yield a new beam $E(x;\alpha)$. The original and 'delayed' beams combine at another beam splitter, and their superposition is integrated by a bucket detector to produce an interferogram. (d,e) Graphical depiction of the matrix form of a generalized interferogram. (d) With evenly spaced Nyquist-rate sampling of the interferogram $M\geq2N$, the interferometric sensing matrix $\mathbf{\Phi}_{\text{int}}$ has a well-defined deterministic structure. (e) With sub-Nyquist randomly sampled points α, $\mathbf{\Phi}_{\text{int}}$ now appears disordered and similar to $\mathbf{\Phi}$ in (b).

Optics EXPRESS

bases are optical realizations of the fractional Fourier transform (FrFT) [49, 50] or fractional Hankel transform (FrHT) [51], respectively. In all cases, the compressive interferometry strategy replaces harmonic analysis of the Nyquist-sampled interferogram with random sub-Nyquist sampling *without* modifying the native optical hardware. By constructing an intrinsically stable, basis-neutral interferometer that includes realizations of fractional transforms [8], we confirm that CS helps successfully reconstruct the modal weights of sparse optical beams in a basis of HG or LG modes from the random sub-Nyquist samples. This may help in delay-intolerant applications that require real-time acquisition and processing, such as real-time imaging and high-speed communications exploiting spatial multiplexing.

A typical optical implementation of CS is depicted in Fig. 1(a) [12, 27, 28]. Consider an optical field $E(x)=\sum_n c_n\psi_n(x)$ represented in an N-dimensional orthonormal basis $\{\psi_n(x)\}$, and $E(x)$ is normalized such $\sum|c_n|^2=1$. Here x may refer to one or more spatial dimensions, or even time. The $N\times1$-vector $\mathbf{x}=\{c_n\}$ of coefficients is s-sparse if it receives contributions from $\leq s$ elements. In lieu of the $M\geq 2N$ Nyquist-rate measurements normally required to reconstruct $\mathbf{x}$, CS leverages sparsity to reduce M by projecting the field onto a sequence of *random masks* selected from a Gaussian ensemble to produce a new $M\times1$ *measurement vector* $\mathbf{y}$. Effectively, the field has undergone a linear transformation represented by an $M\times N$ *sensing matrix* $\mathbf{\Phi}$, $\mathbf{y}=\mathbf{\Phi x}$ [Fig. 1(b)]. CS exploits this under-determined linear system to compressively recover $\mathbf{x}$ from $M\approx O(s\log N)\ll N$ linear measurements of $\mathbf{y}$ – provided some conditions on $\mathbf{\Phi}$ are satisfied. For example, Basis Pursuit (BP) recovers $\mathbf{x}$ if $\mathbf{\Phi}$ satisfies the Restricted Isometry Property (RIP) [10], which requires that $(1-\delta)\|\mathbf{x}\|^2\leq\|\mathbf{\Phi x}\|^2\leq(1+\delta)\|\mathbf{x}\|^2$, for any s-sparse $\mathbf{x}$, where $0<\delta<1$ is a constant. Sensing matrices from Gaussian ensembles, for example, satisfy the RIP with overwhelming probability [10]. The random masks introduce new components into the optical system, thus adding to its complexity while reducing the number of measurements acquired.

The *compressive interferometry* scheme relies on a different strategy. Consider an interferogram $P(\alpha)$ traced by scanning a 'delay' α placed in one arm of a two-path interferometer [Fig. 1(c)]. With respect to the modal basis $\{\psi_n(x)\}$, such a delay is an optical transformation having a continuous real control parameter α, $\Lambda(x,x';\alpha)=\sum_n e^{in\alpha}\psi_n(x)\psi_n^*(x')$, which is a fractional transform having the basis functions as eigenstates with eigenvalues $e^{in\alpha}$, and $\Lambda(x,x';0)=\delta(x-x')$ [2]. The parameter α acts as a 'delay' in the Hilbert space spanned by $\{\psi_n(x)\}$ just as a delay τ does in the time domain. That α is in fact a delay can be readily seen by superposing the delayed field $E(x;\alpha)=\int dx'\Lambda(x,x';\alpha)E(x')=\sum_n c_n e^{in\alpha}\psi_n(x)$ and the reference $E(x;0)$ to produce the interferogram

$$P(\alpha)\propto\int dx\,|E(x;\alpha)+E(x;0)|^2=1+\sum_{n=1}^{N}|c_n|^2\cos(n\alpha). \tag{1}$$

The modal coefficients $\mathbf{x}=\{|c_n|^2\}$ are revealed by taking a Fourier transform (FT) with respect to α. This requires sampling α at the Nyquist rate dictated by the highest-order mode N – even if only a few modes contribute significantly [Fig.1 (d)].

To show that CS algorithms may recover the sparse vector $\mathbf{x}$ from $M\ll N$ measurements, we first cast $P(\alpha)$ from Eq. (1) with *selected values* of α into a linear model. A $M\times N$ interferometric sensing matrix $\mathbf{\Phi}_{\text{int}}$ relates the $N\times1$ vector $\mathbf{x}$ of contributions from each Hilbert-space basis-element to the $M\times1$ measurement-vector $\mathbf{y}$ that contains the sampled interferogram [Fig. 1(e)],

$$\underbrace{\begin{bmatrix}P(\alpha_1)-1\\P(\alpha_2)-1\\\vdots\\P(\alpha_M)-1\end{bmatrix}}_{\mathbf{y}}=\underbrace{\begin{bmatrix}\cos\alpha_1&\cos2\alpha_1&\dots&\cos N\alpha_1\\\cos\alpha_2&\cos2\alpha_2&\dots&\cos N\alpha_2\\\vdots&\vdots&\ddots&\vdots\\\cos\alpha_M&\cos2\alpha_M&\dots&\cos N\alpha_M\end{bmatrix}}_{\mathbf{\Phi}_{\text{int}}}\underbrace{\begin{bmatrix}|c_1|^2\\|c_2|^2\\\vdots\\|c_N|^2\end{bmatrix}}_{\mathbf{x}}. \tag{2}$$

Optics EXPRESS

Here, $\mathbf{\Phi}_{\text{int}}$ corresponds to *any* interferometric measurement, temporal or otherwise.

3. Properties of the sensing matrix

The sparsity of the vector or signal of interest (in some basis) alone does not premise successful recovery in sub-Nyquist sampling regimes using CS-based reconstruction. Establishing performance guarantees for sparse reconstruction also necessitates having an appropriate sensing matrix mapping the sparse vector to the lower-dimensional measurement space. To clarify, consider the simple scenario with measurements $\mathbf{y} = \mathbf{\Phi x}$, where $\mathbf{\Phi} = \mathbf{I}$, the identity matrix. Obviously, in this case one cannot reconstruct an arbitrary sparse vector $\mathbf{x}$ if only few rows of the matrix $\mathbf{\Phi}$ are given. Hence, although the exact $\mathbf{x}$ is readily available from full measurements, we cannot recover $\mathbf{x}$ from few measurements selected at random as we are likely to miss the nonzero entries on the support. Another example is one in which the sparse vector lies in the null-space of the sensing matrix. In this case, recovery is not possible even though the vector is sparse. A classic example from the CS literature where sub-Nyquist sampling also fails despite the sparsity of the signal is when the sensing matrix $\mathbf{\Phi}$ is strongly coherent with the sparsifying basis $\mathbf{\Psi}$ – the basis in which the signal admits a sparse representation – i.e., when the maximum correlation between the rows of $\mathbf{\Phi}$ and columns of $\mathbf{\Psi}$ is large [52]. For instance, a submatrix from the Discrete Fourier Transform (DFT) does not avail substantial compression gains when $\mathbf{\Psi}$ is the Inverse Discrete Cosine Transform (IDCT) matrix given that they have large mutual coherence.

A general rule-of-thumb is that an appropriate matrix for CS should preserve distances between vectors (signals) after the high-dimensional sparse signals are embedded into the lower-dimensional space defined by its range. For example, this property is fulfilled if the sensing matrix satisfies the RIP for $2s$-sparse vectors with a sufficiently small δ. Besides, being RIP implies that none of these sparse vectors falls in the null-space of the sensing matrix.

The sensing matrix $\mathbf{\Phi}_{\text{int}}$ arising in our setup differs fundamentally from those typically employed in CS applications in optics [Fig. 1(a) and 1(b)], where controllably random transformations $\mathbf{\Phi}$ are realized by an array of random patterns that are judiciously selected such that $\mathbf{\Phi}$ has the RIP, for example. In interferometry, this freedom in designing $\mathbf{\Phi}_{\text{int}}$ is not available because $\mathbf{\Phi}_{\text{int}}$ has a *fixed structure* with few controllable degrees of freedom (the values of the delay parameter α) imposed by the constrained sensing structure (the interferometer itself). Hence, it is not clear at the outset if the sensing matrix $\mathbf{\Phi}_{\text{int}}$ satisfies any of the known sufficient conditions for successful CS recovery. Therefore, to decide if sub-Nyquist sampling of the interferogram and CS-based reconstruction will succeed in our setting, it is crucial to investigate the properties of the sensing matrix $\mathbf{\Phi}_{\text{int}}$.

Given the constrained form of $\mathbf{\Phi}_{\text{int}}$ in Eq. (2), it can be shown that selecting random values of α from a uniform distribution at a sub-Nyquist rate yields $\mathbf{\Phi}_{\text{int}}$ that satisfies the RIP with high probability when M and N are sufficiently large. For smaller values of M and N, however, the RIP constant δ is large. The sufficient conditions for all existing reconstruction algorithms require smaller values of δ to guarantee successful reconstruction. For example, a sufficient condition for BP requires $\delta < \sqrt{2} - 1$. Having the large δ associated with $\mathbf{\Phi}_{\text{int}}$ therefore does not guarantee reconstruction on the basis of these requirements. As an illustration, in Fig. 2(a) we plot $\eta(\mathbf{x}) = (\|(\sqrt{2/M})\mathbf{\Phi}_{\text{int}}\mathbf{x}\|^2/\|\mathbf{x}\|^2) - 1$ with a typical realization of the sensing matrix for a subset of an ensemble of 10^6 sparse-vector realizations $\mathbf{x}$ with $s = 4$, where $\max_{\mathbf{x}} |\eta(\mathbf{x})| \leq \delta$. A histogram constructed from the full ensemble is plotted in Fig. 2(b), showing that the requirement of a small enough δ is unsatisfied. While such a requirement may not be necessary, given existing knowledge it is not known if the corresponding bound on δ is tight, i.e., if some performance guarantee can be established with a relaxed RIP constant. Therefore, we resort to verifying a more general RIP-less notion to establish performance guarantees. In particular, we are able to show that the sensing matrix $\mathbf{\Phi}_{\text{int}}$ with randomly selected α indeed belongs to a random ensemble satisfying weaker *incoherence* and *isotropy* properties despite its limited degrees of freedom

Optics EXPRESS

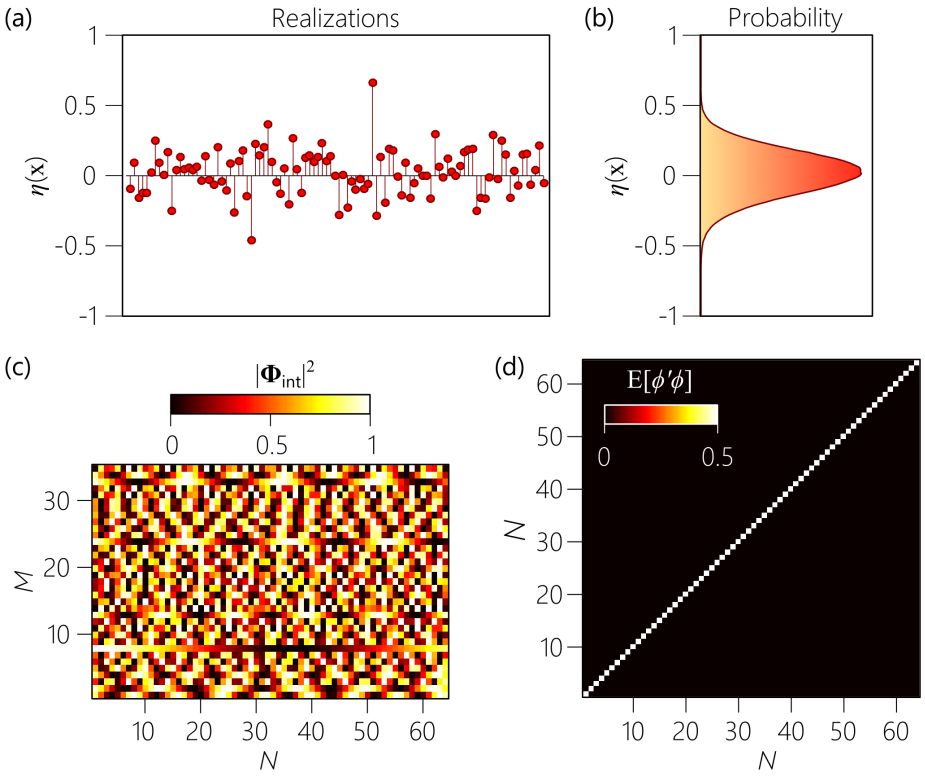

Fig. 2. (a) Calculated values of $\eta(\mathbf{x}) = \|(\sqrt{2/M})\mathbf{\Phi}_{\text{int}}\mathbf{x}\|^2/\|\mathbf{x}\|^2 - 1$ for s-sparse ($s=4$) vectors $\mathbf{x}$. (b) Histogram of $\eta(\mathbf{x})$ for an ensemble of 10^6 realizations of s-sparse vectors. (c) The sensing matrix $\mathbf{\Phi}_{\text{int}}$ from Eq. (2) with randomly sampled α. (d) $\mathbf{\Phi}_{\text{int}}$ is *incoherent* with incoherence parameter $\mu = 1$ and satisfies the *isotropy* property $\text{E}\{\boldsymbol{\phi}^\dagger\boldsymbol{\phi}\} = 0.5\,\mathbf{I}$.

imposed by the interferometric process. Provably, such matrices also yield explicit reconstruction guarantees via BP or other recovery algorithms such as the Dantzig selector or LASSO [53].

To clarify, let $\boldsymbol{\phi}$ denote a row of the sensing matrix selected from a random ensemble $\mathcal{F}$. The *incoherence* parameter $\mu(\mathcal{F})$ is defined as the smallest number for which $\max_n |\phi_n|^2 \le \mu(\mathcal{F})$, $n = 1, 2, \ldots, N$, where ϕ_n are the entries of $\boldsymbol{\phi}$. The distribution $\mathcal{F}$ is said to obey the *isotropy* property if $\text{E}[\boldsymbol{\phi}^\dagger\boldsymbol{\phi}] = a\mathbf{I}$, where E[.] is the expected value, $\mathbf{I}$ the identity matrix, a some constant, and $\boldsymbol{\phi}^\dagger$ the conjugate transpose of $\boldsymbol{\phi}$. The matrix $\mathbf{\Phi}_{\text{int}}$ satisfies the conditions of incoherence and isotropy for α randomly selected from a uniform distribution over $[0, 2\pi]$ with $\mu = 1$, as confirmed in Fig. 2(c) that shows $\mathbf{\Phi}_{\text{int}}$ consisting of M rows selected from the full matrix in Fig. 1(d). The matrix appears random in spite of being sampled from a structured sensing system. The matrix $\mathbf{\Phi}_{\text{int}}$ is shown to satisfy the isotropy property in Fig. 2(d).

4. Experimental results

We now move on to implementing the compressive interferometric scheme experimentally. The generalized delay transformation $\Lambda(x, x'; \alpha)$ has the modal basis $\{\psi_n(x)\}$ as eigenfunctions and its order parameter α represents the delay in the Hilbert space spanned by this basis. We carry out our experiments using two modal bases, 1D HG functions and radial LG functions. The delay transformations $\Lambda(x, x'; \alpha)$ in these two modal bases correspond to the FrFT [49, 50] and the FrHT [51], respectively [2, 3]. The usual temporal delay is replaced with an optical realization of

Optics EXPRESS

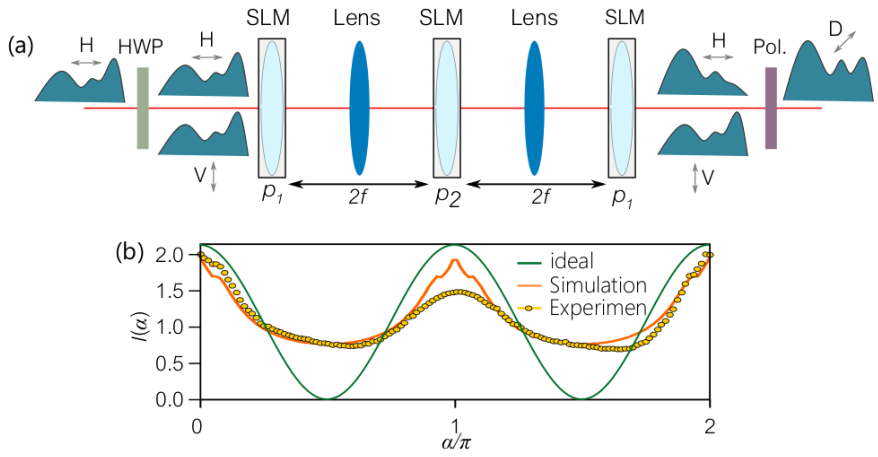

Fig. 3. (a) Implementation of the sampling system as a common-path interferometer leveraging the polarization-selectivity of liquid-crystal-based SLMs. (b) Interferograms collected by assigning different values to the generalized delay parameter α when HG_2 is the only active mode. The figure shows three interferograms collected by an ideal frFT, a simulation that accounts for the pixelation and quantization effects of the SLMs, and the actual experimental setup.

the appropriate fractional transform, whose order α is swept in the interval $[0, 2\pi]$ to produce an interferogram $P(\alpha)$. We construct these fractional transforms using spatial light modulators (SLMs) that realize generalized cylindrical or spherical lenses to produce the FrFT or FrHT, respectively, of desired order [54].

4.1. Experimental setup

The optical beam used in our experiments is provided by a laser diode at 808-nm wavelength. We spatially filter the beam by first coupling it into a single-mode fiber (Thorlabs, FS-SN-4224) followed by collimation and then size-control using a variable beam expander (Thorlabs, BE02-05-B) to produce a Gaussian beam with a full-width at half-maximum of 0.6-mm at the entrance of the optical system.

Note that the FrFT (and by implication also the FrHT) can be implemented via a sequence of lenses. The order of the fractional transform can then be varied either by fixing the focal lengths of the lenses but varying their relative separation, or alternatively by fixing their separation and varying their focal lengths (so-called generalized lenses). In our experiment, we exploit the latter approach and make use of SLMs to implement a lens by realizing the appropriate quadratic phase distribution. We use the same realization of the FrFT and FrHT that we reported on in Ref. [8] that requires three SLMs – p_1, p_2, and p_3 in Fig. 3(a). Because the first and last SLMs p_1 and p_3 realize the same lens, the number of SLMs required can be reduced to two by exploiting a reflection configuration in which p_3 is folded back onto p_1. These reflection-mode SLMs were Hamamatsu LCOS-SLM (X10468-02) having 800×600 pixels, an effective area of 16×12 mm^2, and 256 quantized phase levels (8 bits). The angle of incidence on SLM p_1 is < 10 deg, the reflected beam is directed to SLM p_2 at normal incidence. The retro-reflected beam again impinges on SLM p_1 and then imaged to the detector plane. The phases implemented by the SLMs are designed to implement cylindrical or spherical lenses that in combination produce the FrFT or FrHT, respectively, of the desired order.

Instead of placing this realization of the FrFT or FrHT in one arm of a Mach-Zehnder interferometer as shown in Fig. 1(c), we exploit a different interferometric setup that is intrinsically

Optics EXPRESS

stable by exploiting the polarization-selectivity of liquid-crystal-based SLMs [55] to create a common-path interferometer. The input beam is horizontally polarized and the SLMs modulate the horizontal polarization only – which thus undergoes the generalized delay – while the vertical polarization represents the reference. A common-path polarization interferometer is then configured by first rotating the input polarization via a half-wave plate from horizontal to 45 deg. At the output a polarization projection superposes the reference and the delayed beams into a single polarization mode and yields the generalized interferogram as the delay is swept.

Finally, since the vertically polarized reference field is not impacted by the SLMs, it undergoes diffraction resulting from free-space propagation from the entrance of the setup to the exit, which is undesirable. We thus place two lenses (focal length of each is $f = 500$ mm) in a $4f$ imaging configuration that maps the entrance plane to the exit, thus eliminating this unwanted diffraction. The phases implemented by the SLMs are then modified to retain the targeted orders of the FrFT and FrHT. At the output, an image of the beam at the output of the common-path interferometer is recorded for each value of the generalized delay by a CCD camera (The Imaging Source, DFK 72BUC02). The setup implemented is shown schematically in Fig. 3(a); see Ref. [8] for details.

4.2. Results

In the compressive interferometry approach, α is randomly sampled at a sub-Nyquist rate. We study the performance of this strategy by comparing the modal reconstruction in the HG and radial LG bases to that obtained via the FT. M measurements are collected randomly by selecting generalized phases α_j, $j = 1, 2, \ldots, M$ from a uniform random distribution $[0, 2\pi]$, and we use the BP algorithm to reconstruct the vector $\tilde{\mathbf{x}}$ of modal coefficients. The reconstructed vector is then compared to the vector $\mathbf{x}_{\mathrm{FT}}$ obtained from the FT of 128 uniformly sampled interferometric measurements by computing the scaled error metric, $||\mathbf{x}_{\mathrm{FT}} - \tilde{\mathbf{x}}||_2^2 / ||\mathbf{x}_{\mathrm{FT}}||^2$. For each example, the average reconstruction error is evaluated by averaging over 100 runs. The number of potential modes is $N = 64$. Figures 4(a) and 4(b) show the reconstructed modal coefficients using FT and CS for input beams formed from individual HG or LG modes, respectively. In Fig. 4(c), we plot the reconstructed modal coefficients for two beams formed of different superpositions of HG modes. The performance of the BP algorithm is comparable to that of FT using $M = 30$ compressive measurements ($\approx 25\%$ of the measurements in FT), leading to substantial savings in acquisition time without any added complexity to the system. The reconstruction error is plotted in Fig. 5 (a) as a function of M. The average error approaches zero when $M \approx 25$. Statistical analysis of the observed error reveals that the required number of measurements lies between $M = 15$ to $M = 30$ to attain nearly error-free reconstruction. Fig. 5 (b) compares the reconstruction error achieved in the experiment to that obtained from numerical simulation as a function of the number of measurements for the HG_3 mode. As shown, the experiment and simulation results exhibit a fairly close agreement. The discrepancy in the error floor at convergence is due to limitations of the SLMs unmodeled in our simulations (c.f. discussion in Sec. 5 on practical limitations.)

5. Discussion

Two-dimensional (2D) modal analysis: In this work, we investigated the performance of the proposed compressive interferometry approach in analyzing a light beam based on 1D HG and LG modes, however, our approach extends naturally to 2D settings with two degrees of freedom. For further details, we refer the reader to [32], where we investigated (in theory) compressive analysis of a light beam in two sets of HG modes (HG-HG modes) with two (Cartesian) spatial degrees of freedom, and also Orbital Angular Momentum (OAM) and LG modes (OAM-LG modes) with angular and radial degrees of freedom. It has been shown that 2D modal analysis can be achieved by cascading two generalized delays (phase operators) in the reference arm of the interferometer corresponding to each degree of freedom. For example, to analyze an incident

Optics EXPRESS

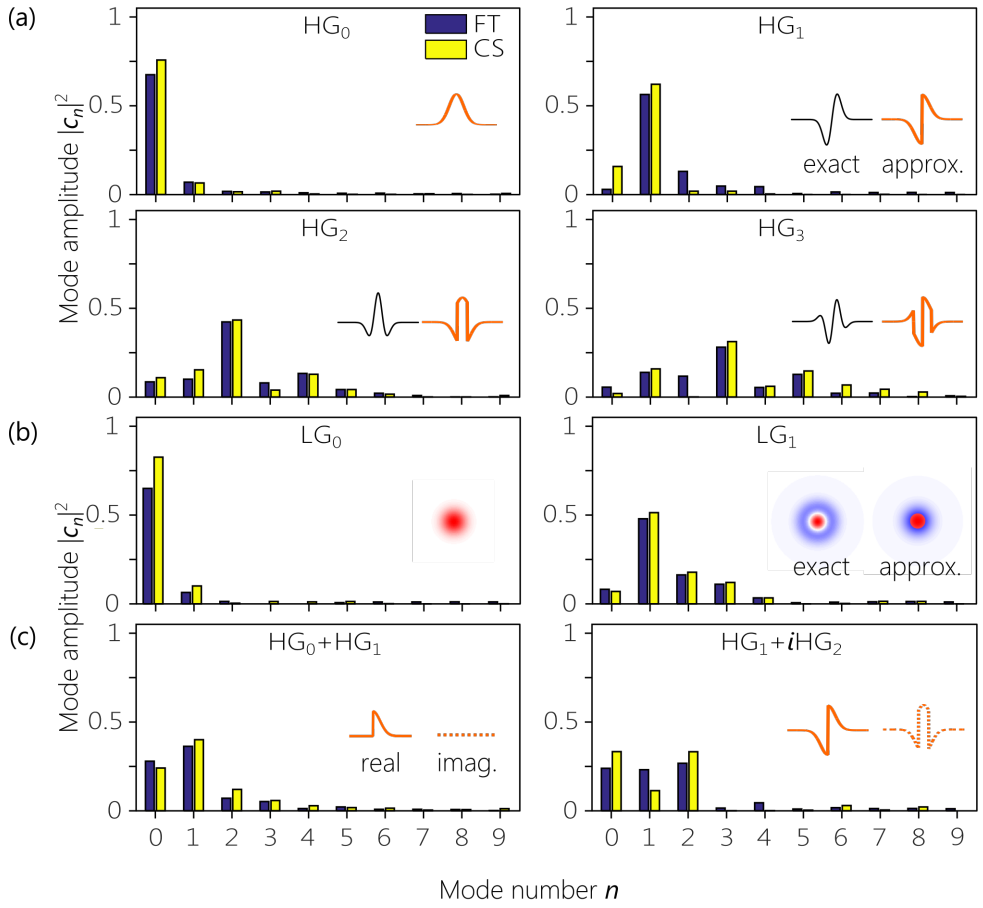

Fig. 4. Reconstructed modal distributions using the FT and CS approaches. (a) The modal weights $|c_n|^2$ calculated for fields in the HG-basis by applying the FT to Nyquist-rate evenly sampled interferograms (blue) and CS to sub-Nyquist randomly sampled (yellow) interferograms. (b) Same as (a) for LG modes (LG_0 and LG_1) and (c) for superposition of HG modes (HG_0+HG_1 and $HG_1 + iHG_2$). For FT, we use 128 evenly spaced values of α from 0 to 2π. For CS, we use $M = 30$ randomly selected $\alpha \sim \mathcal{U}[0, 2\pi]$. The insets show the ideal (exact) and approximated modes that are implemented experimentally. For HG_0 and LG_0, the modes are produced without approximation.

light beam in its OAM-LG modes, the reference arm of the interferometer is realized by a rotation operator followed by a fractional Hankel transform.

Practical limitations: Due to practical considerations, there exist several sources of inaccuracy that affect the quality of the measurements collected, which could in turn lead to some degradation in modal reconstruction. One is due to the use of inexact (non-ideal) optical modes in the experiments shown in the insets of Fig. 4 (see Ref. [8] for more details on the generation of such modes). As such, even if the incident light beam consists of a single mode, it will have non-vanishing (albeit small) projections on the rest of the elements of the modal basis (in addition to the dominant mode) due to loss in orthogonality. Hence, the coefficient vector $\mathbf{x}$ typically contains small nonzero entries for the various modes in addition to the dominant entries corresponding to the active modes. Such vectors are referred to as 'compressible' vectors since they are not exactly 'sparse'. A second source of inaccuracy is due to noise, usually modeled as additive noise, i.e.,

Optics EXPRESS

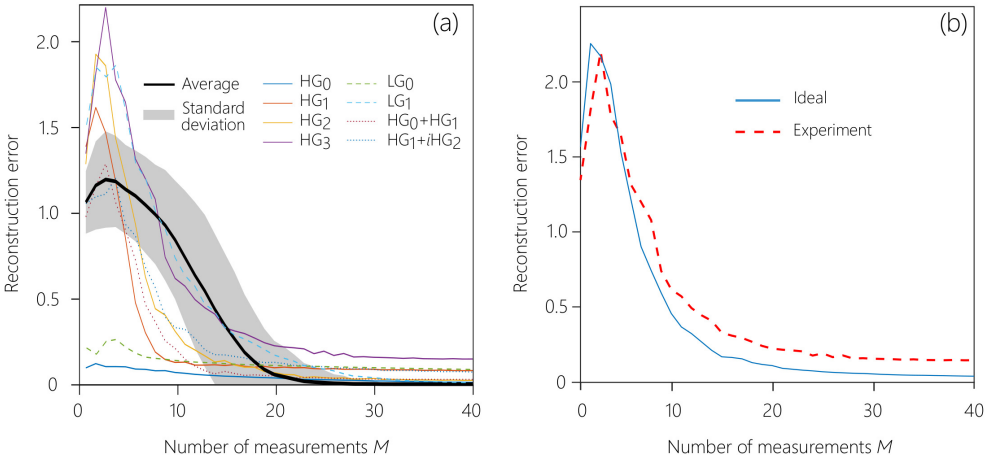

Fig. 5. (a) Reconstruction error versus number of measurements M. Each curve results from averaging over 100 runs of the experiment. The average curve (solid black) is the mean and the shaded area designate one standard deviation spread on either side of the required M for 1000 randomly generated examples of sparse vectors with support size $s \leq 4$. (b) Comparing the reconstruction error in the experiment to that of the ideal case with an approximate HG_3 mode for SNR= 20 dB.

$\mathbf{y} = \mathbf{\Phi}_{\text{int}}\mathbf{x} + \mathbf{n}$, where $\mathbf{n}$ is an additive noise vector with bounded ℓ_2-norm. While denoising algorithms (e.g., denoising BP [10], Dantzig selector [56]) could be used to enhance performance, such algorithms typically require additional side information about the noise (for example, a reliable upper bound on its ℓ_2-norm) to enhance the stability of the solution given the loss in SNR. Unfortunately, such side information is generally hard to obtain in practice. Another source of inaccuracy is due to unavoidable physical constraints and hardware limitations. Specifically, limitations include the clipping effect due to the finite-aperture size of the SLMs, limited spatial resolution of the phase on the SLMs due to their non-vanishing pixel size, and phase granularity due to the finiteness of the number of phase quantization levels (c.f. [8] for further details). As shown in Fig. 3(b), the actual interferometric measurements do not perfectly agree with the ideal measurements due to such imperfections. This figure also displays simulation results where we partially account for the effects of clipping and SLM pixelation improving the agreement between the experimental and numerical results. These imperfections typically manifest themselves in the measurement model non-linearly, and an exact analysis of the performance bounds accounting for such imperfections remains elusive.

Peformance bounds: The reconstruction error does not necessarily converge to zero as we increase the number of measurements as seen in Fig. 5 (a) (e.g., the HG_3 mode). Inexact reconstruction can be foreseen based on [53, Theorem 1.3], which provides an upper bound on the reconstruction error under an additive noise model in terms of the variance of the noise and the norm of the residual error from the best s-sparse approximation of the (compressible) vector $\mathbf{x}$ given the incoherence and isotropy properties. However, predicting an actual (tight) upper bound from the theory is prohibitive in our non-ideal experimental setting since neither is knowledge of the variance of the noise and the residual error at our disposal, nor do we have an exactly additive noise model (due to the aforementioned non-linearities from hardware limitations).

Complexity analysis: The proposed compressive interferometry approach requires sampling a number of measurements M of order $O(s \log N)$ versus $O(N)$ for Nyquist sampling. This signifies substantial saving in data collection time, especially for sufficiently large problem sizes. For

Optics EXPRESS

decoding, a separate processor is used to run a fast algorithm to recover the modal content from collected interferometric measurements. For simplicity, in this paper we have used Basis Pursuit (BP) as our algorithm of choice, however, faster recovery algorithms (such as Orthogonal Matching Pursuit [57]) known to run in nearly linear time $O(NM)$ could also be adopted. Since $M = O(s \log N)$, the decoding complexity of such algorithms is of the same order of $O(N \log N)$ for FFT for small s (sparse beams). We remark that BP (which relies on standard LP relaxation) still runs in favorable polynomial time, which suffices for our purpose since we are not dealing with excessively large problem sizes. Thus, the reduction in processing time, which combines both the sampling and decoding times, is mostly proportional to the saving in sample size complexity, which is considerable in regards to scaling laws.

6. Conclusion

In conclusion, we have devised a compressive approach to interferometry whereby the modal content of light beams can be recovered by sampling intereferograms randomly at sub-Nyquist rate using native optics hardware, which was demonstrated experimentally. Two fundamental differences distinguish our strategy from prior work employing CS in optics. First, the interferometric sensing matrix is imposed through the structure of the interferometer. As such, compression has to be carried out under sensing constraints enforced by the limited degrees of freedom of the sensing system. Second, previous work in the context of interferometry focused on reducing the number of measurements used for reconstruction, but not on *compressive data acquisition*. By leveraging the notion of generalized delay, our approach enables compressive modal analysis in an arbitrary modal basis. Furthermore, we established provable guarantees for successful reconstruction despite the sensing constraints set by the limited degrees of freedom of the interferometer.

Funding

Office of Naval Research (ONR) contracts N00014-14-1-0260 and N00014-17-1-2458; National Science Foundation (NSF) CAREER Award CCF-1552497.